

FREEFORM OPTICS POST-PROCESSING
USING PSEUDO-RANDOM ORBITING STROKE

by

Xiangyu Guo

Copyright © Xiangyu Guo 2018

A Thesis Submitted to the Faculty of the

COLLEGE OF OPTICAL SCIENCES

In Partial Fulfillment of the Requirements

For the Degree of

MASTER OF SCIENCE

In the Graduate College

THE UNIVERSITY OF ARIZONA

2018

THE UNIVERSITY OF ARIZONA
GRADUATE COLLEGE

As members of the Master's Committee, we certify that we have read the thesis prepared by *Xiangyu Guo*, titled *Freeform Optics Post-Processing Using Pseudo-Random Orbiting Stroke* and recommend that it be accepted as fulfilling the thesis requirement for the Master's Degree.



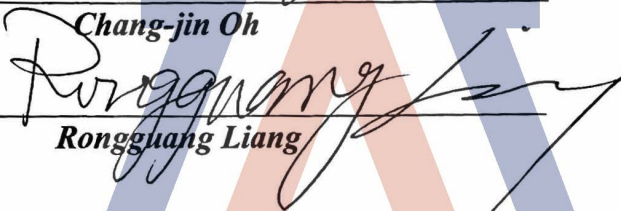
Dae Wook Kim

Date: (11/13/2018)



Chang-jin Oh

Date: (11/13/2018)



Rongguang Liang

Date: (11/13/2018)

Final approval and acceptance of this thesis is contingent upon the candidate's submission of the final copies of the thesis to the Graduate College.

I hereby certify that I have read this thesis prepared under my direction and recommend that it be accepted as fulfilling the Master's requirement.





Date: (11/13/2018)

Dae Wook Kim
Associate Professor
Optical Sciences and Astronomy

ARIZONA

ACKNOWLEDGEMENTS

I would like to first thank my parents in China for their support that encouraged me to pursue Master's degree abroad. I am very grateful to my adviser, Dr. Dae Wook Kim. This project would not have been possible without his constant support and mentoring. I also appreciate my lab members and opticians who work for OEFF, they taught me a lot on not only knowledge but also experience in life. I would also like to acknowledge the members of my committee, Dr. Chang-jin Oh and Dr. Rongguang Liang, who took their time to review this thesis and gave me valuable suggestions.

In addition, this research was made possible by the Korea Basic Science Institute Foundation.

DEDICATION

To my parents: Yingfu and Haiyan

LIST OF CONTENTS

LIST OF FIGURES	7
LIST OF TABLES	9
ABSTRACT	10
1 INTRODUCTION	11
1.1 Thesis Content	12
2 FREEFORM OPTICS FABRICATION METHODS	14
2.1 Freeform Optics	14
2.2 Traditional Optics Manufacturing	15
2.3 Single-Point Diamond Turning (SPDT)	16
2.4 Magneto-Rheological Finishing (MRF)	18
3 PROS FREEFORM POST-PROCESSING TECHNIQUE	20
3.1 Preston's Equation	20
3.2 PROS Post-Processing Interface Material	21
3.2.1 Post-Processing Lap/Tool	21
3.2.2 Polishing Compound and Slurry	25
3.3 Small Stroke CNC Pseudo-random Orbiting Stroke	28
4 CNC PROS MACHINE AND SOFTWARE	34
4.1 CNC Machine Configuration	34
4.2 Mach 3 Software and G Code	35

5	EXPERIMENTAL SETUP AND METROLOGY CONFIGURATION.....	38
5.1	PROS Post-processing Experiment Setup.....	38
5.2	Measurement Configuration for Data Acquisition.....	39
4 inch	40
6	FREEFORM OPTICS POST-PROCESSING PERFORMANCE	43
6.1	Surface Form Preservation Analysis	43
6.2	Analysis of Micro-Surface Roughness Improvement	44
7	CONCLUSION.....	49
	REFERENCES	50

LIST OF FIGURES

Figure 1 Three examples of freeform optics ¹¹	15
Figure 2 Strasbaugh machine (left) and the sketch for the mechanism (right)	15
Figure 3 4-axis diamond turning machine configuration. ¹⁷	17
Figure 4 MRF lens manufacturing set up (left) and the schematic sketch of MRF fabrication and polishing mechanism (right). ²²	18
Figure 5 Ideal post-processing using PROS process, which removes a uniform layer of materials (i.e., nominal removal depth) while maintaining the original surface profile and improves the high spatial frequency surface finish.....	20
Figure 6 Gugolz #63 and #73 pitch.....	22
Figure 7 SEM microphotograph (left) and texture (right) of LP-66 polishing pad ²⁹	23
Figure 8 SEM microphotograph (left) and texture (right)of Black CHEM2 polishing pad . ³⁰	24
Figure 9 Pitch tool pressing process.	24
Figure 10 Pitch lap with channels.	25
Figure 11 Rhodite 906 polishing powder. ³²	26
Figure 12 Linde B alumina compound. ³³	27
Figure 13 Top view of the directional experiment setup.	28
Figure 14 Surface profile comparison: PSD against (left) and along (right) directional smoothing process.	30

Figure 15 Schematic showing the geometrical relationship between the workpiece and tool (left) and the PROS tool path generated using the CNC machine control software (right).	32
Figure 16 Schematic of the PROS process CNC setup.....	35
Figure 17 User-interface of Mach 3 control software. ³⁸	36
Figure 18 VeriFire™ interferometer used for the PROS process experiments.	40
Figure 19 NewView white light interferometer used for the PROS process experiments in the lab.....	42
Figure 20 Measured full aperture maps using VeriFire™ interferometer for the initial and smoothed stages, and the corresponding subtracted surface map showing the difference between the before and after the PROS process.....	44
Figure 21 Micro-surface roughness comparison of all samples.	45
Figure 22 Distribution of measured micro-surface roughness (Ra) against various states. The bars and curves stand for the micro-surface roughness distribution and fitted curve in each state, respectively.	46
Figure 23 Analyses of linear profile data (left) and PSD (right) for the SPDT PMMA and Al6061 samples before and after the PROS post-processing.	47
Figure 24 Visual appearance of the Al6061 sample before (left) and after (right) the smoothing process.	48

LIST OF TABLES

Table 1 Gugolz polishing pitch technical data. ²⁸	22
Table 2 LP-66 polishing pad properties. ²⁹	23
Table 3 Rhodite 906 technical data. ³¹	26
Table 4 Linde B technical data. ³³	27
Table 5 Roughness parameters PV and Ra for each surface profile in each smoothing process.	31
Table 6 Key features in PROS post-processing technique.	33
Table 7 machine specification. ³⁷	34
Table 8 G Code examples. ³⁹	37
Table 9 Description of the initial states of the BK7, PMMA, and Al6061 workpieces. ..	38
Table 10 Post-processing information of the BK7, PMMA and Al6061 workpieces.	39
Table 11 Specification data of the ZYGO VeriFire™ interferometer. ⁴⁰	40
Table 12 Measurement patterns for three experiments.	41
Table 13 Specification data of the NewView 8000 white light interferometer. ⁴¹	41
Table 14 Measurement setup parameters for the white light interferometer.	42
Table 15 Full aperture PV and RMS comparisons of the initial, smoothed, and subtracted maps for BK7, PMMA and Al6061.	43
Table 16 Smoothing times for each stage for BK7, PMMA, and Al6061.	45

ABSTRACT

In addition to achieving a desired freeform profile, ensuring superb micro-roughness finish is a key factor for a successful freeform optics manufacturing. We present a Pseudo-random Orbiting Stroke (PROS)-based post-processing technique that maintains freeform optics forms while improving small-scale surface quality. The full aperture tool can avoid subaperture effects, and the small stroke pseudo-random tool path guarantees the match of freeform profiles while preventing the directionality of the final surface profiles. Three independent experimental studies are designed, conducted, and presented for a wide range of optics, including magnetorheological finishing (MRF)-polished BK7 glass, single-point diamond-turned (SPDT) polymethylmethacrylate (PMMA), and SPDT Al6061 optics. The comparison of direct measured maps on the initial and final smoothed optics verifies the form maintenance capability of the freeform optics post-processing technology. Surface roughness measurement highlights improvements in local surface roughness and periodic tool mark errors left by the previous polishing method.

Important Note: Most parts of this MS thesis is directly based on a journal manuscript¹ “Pseudo-random orbiting stroke for freeform optics post-processing,” which is prepared and planned to be submitted to an optical engineering journal. In order to make this MS thesis self-sufficient, additional materials and data have been added to the journal manuscript’s contents.

1 INTRODUCTION

One significant characteristic of freeform optics is that the local radius of curvature varies across the surface. Thus, imperfect matching between the tool and optical surface under fabrication will cause non-uniform pressure distribution and lead to local or zonal surface figure errors. Although opticians often prefer large rigid tools, which induce fewer small-scale errors, to accommodate the locally varying aspheric/freeform optics and to correct localized surface errors more rapidly, they utilize small tools with a computer-controlled tool path to fabricate such non-spherical optics.^{1,2} However, due to the uncertainties in the material removal rate and regular tool path, the subaperture figuring process using a small tool can generate mid-to-high spatial frequency errors on the surface. Apart from that, a more adaptable method known as single-point diamond turning (SPDT) was developed and widely used by the precision optical manufacturing community since the 1970s,³ especially for soft ductile materials. However, the existence of mid-to-high spatial frequency errors continues to be a problem.

To overcome the weakness of the traditional subaperture polishing tool, Kim and Burge proposed a rigid conformal (RC) tool,⁴ which combined a non-Newtonian fluid with traditional polishing pads to obtain a balance between freeform conformability and smoothing rigidity. Another noteworthy development concerns the field of tool path control and optimization. To restrain small tool footprint marks and minimize the mid-to-high spatial frequency errors, new tool paths are applied to replace regular raster and spiral paths. Zeeko Ltd.'s "precessions"⁵ developed the unicursal path, and Tam et al.⁶ presented peano-like paths in 2013. Finishing processes such as ion beam finishing (IBF)⁷ and magnetorheological finishing (MRF)⁸ are also used, and even though the well-controlled

IBF and MRF may not generate mid-to-high spatial frequency errors, another smoothing process is often required to achieve better surface quality.

A post-smoothing process can be applied to further decrease the mid-to-high spatial frequency errors while achieving the desired freeform surface figure and better surface quality conveniently. OPTIMAX invented and matured a proprietary VIBETM technology,⁹ which is a full-aperture high-speed computer-controlled surface smoothing process. This technology has been successfully applied and demonstrated to rapidly post-smooth aspherical or freeform optics with a high surface quality, but the technical details have not been reported caused by its proprietary nature as a key technology of OPTIMAX.

Inspired by the VIBE approach and aiming at both maintaining the desired freeform optical surface figure and decreasing the high spatial frequency surface errors (i.e., surface roughness) for various optical materials and freeform manufacturing methods, we developed a Pseudo-random Orbiting Stroke (PROS) Computer Numerical Control (CNC) post-processing technique, which can be applied to varied optics sizes, materials, and pre-polishing methods. Three representative experimental case studies using freeform optics made out of glass (BK7), plastic (Polymethylmethacrylate or PMMA), and aluminum (Al6061) for diameters ranging from 30 mm to 100 mm are presented to prove the performance of the proposed post-processing technique.

1.1 Thesis Content

Section 2 provides the concept of the freeform optics and fabrication methods. Two CNC based widely used freeform optics fabrication methods, single-point diamond turning (SPDT) and magnetorheological finishing (MRF), are introduced.

Section 3 describes the key features to the PROS post-processing technique. Specifications and data on common fabrication materials like pitch lap, pads, polishing compounds are given. All the fabrication parameters like pressure, velocity, as well as the materials for the PROS experimental case study are presented in detail. To achieve the goal of the PROS post-processing technique, a specific discussion on the pseudo random orbital stroke tool path is also described in this part.

The CNC machine and its control software are described in Section 4. We provide the PROS experimental setup and metrology configuration in Section 5. Also, the specification data for each freeform optics sample and measuring instruments are offered.

In Section 6, the final performance of the PROS post-processing is evaluated and analyzed. It separates into three parts, the maintenance on the full aperture surface form, micro-surface roughness improvement, and PSD (Power Spectral Density) analysis on the processed SPDT optics. Finally, a conclusion that summarizes this thesis is given in Section 7 along with the limitation and future works.

2 FREEFORM OPTICS FABRICATION METHODS

2.1 Freeform Optics

Freeform surfaces can be defined as surfaces with no axis of rotational invariance (within or beyond the part), and may appear to have arbitrary shape, and regular or irregular surface structures.¹⁰ Comparing to traditional optical components, freeform optics has the following features:¹⁰

1. Increased range of manufacturable surfaces, giving optical designers more flexibility and scope for innovation.
2. Enhancing the optical system performance to the maximum extent. For instance, freeform optics enable optical performance otherwise impossible, such as simultaneously correcting aberrations, increasing depth of field and expanding field of view.
3. Simplifying system structure with fewer surfaces, lower mass, lower cost, smaller package-size and reduced stray-light.
4. Realizing system integration easily, and reducing the difficulty in assembly. For example, multiple optical surfaces can be made on one freeform element.

Freeform optics enables and offers wide application markets in various fields, like green energy, illumination and biomedical engineering. However, Freeform optics also offers challenges for optics manufacturing and measurement. Some examples on the form of freeform optics are in Figure 1.



Figure 1 Three examples of freeform optics¹¹.

2.2 Traditional Optics Manufacturing

In traditional optics manufacturing, the optic is created by lapping the correct radius using dedicated tooling, followed by pitch polishing in a slow iterative process.¹² Figure 2 describes the mechanism of Strasbaugh machine, which is the most frequently used traditional optics fabrication machine.

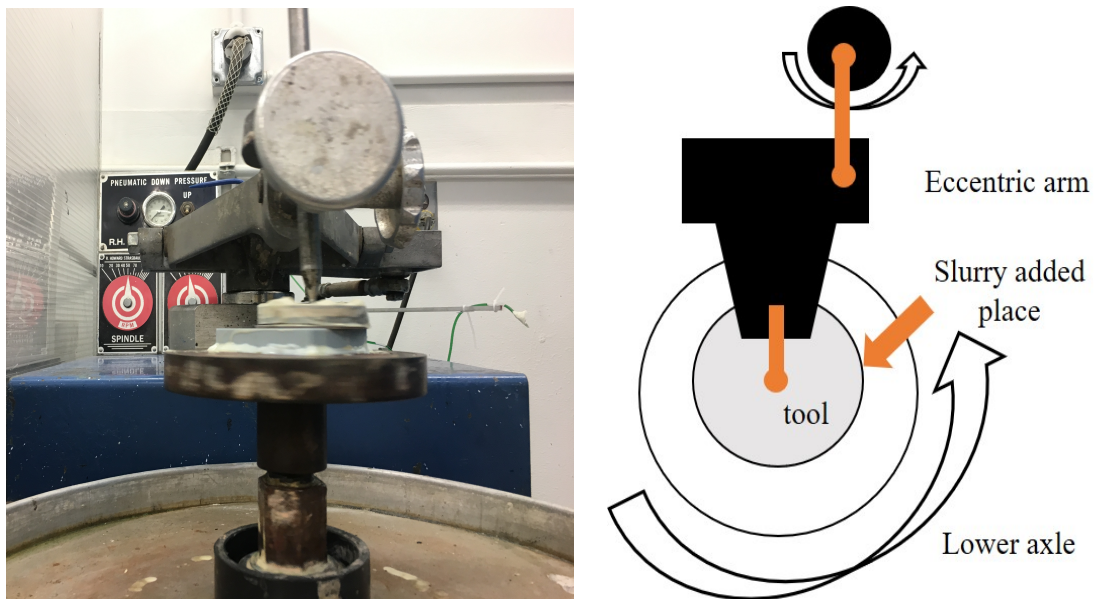


Figure 2 Strasbaugh machine (left) and the sketch for the mechanism (right).

The machine mechanism¹³ is explained as follow. The lower axle rotates and drives the workpiece (or the tool), and an eccentric arm extending a spindle pin that oscillates laterally over the lower axle. The tool (or the workpiece) spins about this pin as it is stroked across the lap. Adjustments include lateral and forward offset of the pin midpoint, length of eccentric stroke, frequency of stroke, and RPM (Revolutions per Minute) of the lap. This method works perfect for symmetric optical surface but is not ideal for asymmetric optics application.

Finally, the introduction of CNC optics manufacturing replaced the need for specialized tooling and created a more deterministic process.¹⁴ Precision optics manufacturing field is dominated by the CNC based optical manufacturing methods at present. The single-point diamond turning (SPDT) and the magnetorheological finishing (MRF) are two classifications of the CNC optics manufacturing.

2.3 Single-Point Diamond Turning (SPDT)

Diamond turning is a process of mechanical machining of precision elements using lathes or derivative machine tools (e.g., turn-mills, rotary transfers) equipped with natural or synthetic diamond-tipped tool bits, and the term single-point diamond turning (SPDT) is sometimes applied.¹⁵

Figure 3 shows the simple diagram of a 4-axis diamond turning machine configuration. The X axis is the feeding direction, Y axis controls the height of the workpiece, the Z axis is the infeed direction, and the C axis (not marked in the figure) is the turning direction of the spindle.¹⁵

As shown in the right side of the figure 3, a nozzle is placed besides the diamond tool.¹⁵ The diamond turning process is often restricted to certain materials. Materials that

are readily machinable include metals (except ferrous metals, which can react with the carbon in the diamond tool), plastics, and infrared crystals.¹⁶ While cutting metal, cooling liquid must be used to cool the contact point. Aluminum alloy is one of the commonly diamond-turned metal materials. Aluminum is a soft and easily oxidized and hard to apply conventional polishing methods.

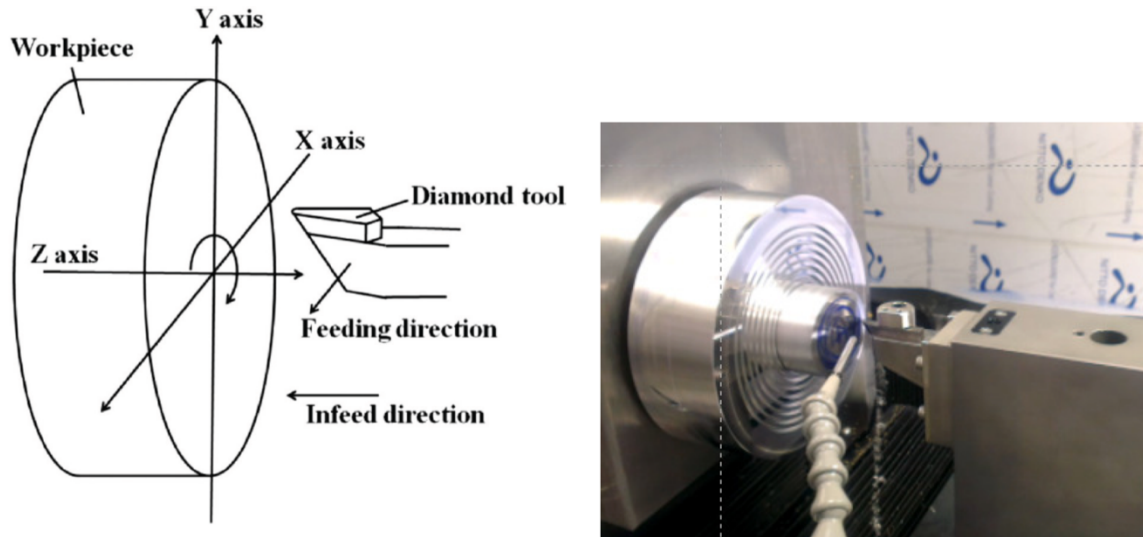


Figure 3 4-axis diamond turning machine configuration.¹⁷

When cutting plastics, however, the liquid could cause damages, so only air is used. The commonly used plastic material is polymethylmethacrylate (PMMA) or acrylic. Advantages of this material is low cost, easy mold-ability into any shape, high light transmission, “green” material characteristics and high UV transmittance.¹⁸ However, a simple post-processing attempt to improve the final surface finish using conventional polishing processes usually result in scratching, embedding of abrasive particles, or forming the “orange peel”.¹⁹

2.4 Magneto-Rheological Finishing (MRF)

Magneto Rheological Finishing (MRF) is a recent finishing technology developed by University of Rochester. This process has a stable and well characterized removal function programmed into a computer. The fluids are magnetic suspensions made of particles with high permeability dispersed in a viscous or viscoelastic non magnetizable medium.²⁰ When subjected to a magnetic field, the fluid greatly increases its apparent viscosity, to the point of becoming a viscoelastic solid.²¹ An example of a lens manufacturing setup using MRF and the schematic mechanism is shown in figure 4.

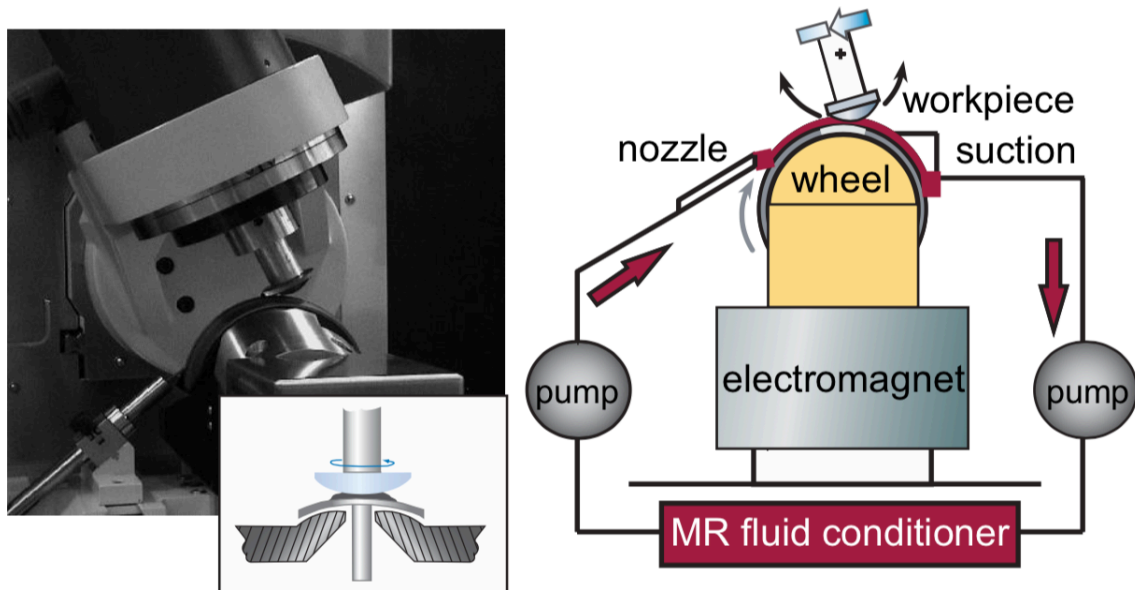


Figure 4 MRF lens manufacturing set up (left) and the schematic sketch of MRF fabrication and polishing mechanism (right).²²

Slurry runs over a belt on a spinning wheel and the lens is lowered into the slurry from above, and the computer can change the hardness of the slurry by controlling the magnet field beneath the spinning belt.²¹

MRF overcomes some common problems of classical polishing approaches because:²²

1. The MRF polishing tool never dulls or changes.
2. The polishing tool works and conforms on complex shapes because it is a fluid.
3. Removal rates are high resulting in short overall processing times.

A notable feature²¹ of MRF is that polishing is driven by shear forces. Thus, the pressure term of Preston's equation in conventional polishing is less significant. When coupled with on-machine interferometry and CNC control, this feature enables high convergence on any desired figure or transmitted wavefront from any (pre-polished) starting shape. Subsurface damage is also greatly reduced, resulting in a high laser damage threshold optics. Print-through effect is also minimized.

In summary, this Section introduced the freeform optics concept and the characteristics of two freeform optics fabrication methods, single-point diamond turning (SPDT) and magneto-rheological finishing (MRF). These two methods offer us practical methods towards hard fabricated materials. By applying SPDT and the MRF, desired freeform profiles can be achieved. These are pre-polishing methods of our experimental study samples in the following Sections.

3 PROS FREEFORM POST-PROCESSING TECHNIQUE

An ideal smoothing process should keep the original freeform surface profile while improving the local surface roughness quality. The goal of the PROS technique is the same. With the characteristic of the full aperture smoothing, the expected removal depth across the entire aperture of the optics should be uniform. The schematic of the PROS post-processing effect is presented in Figure 5.

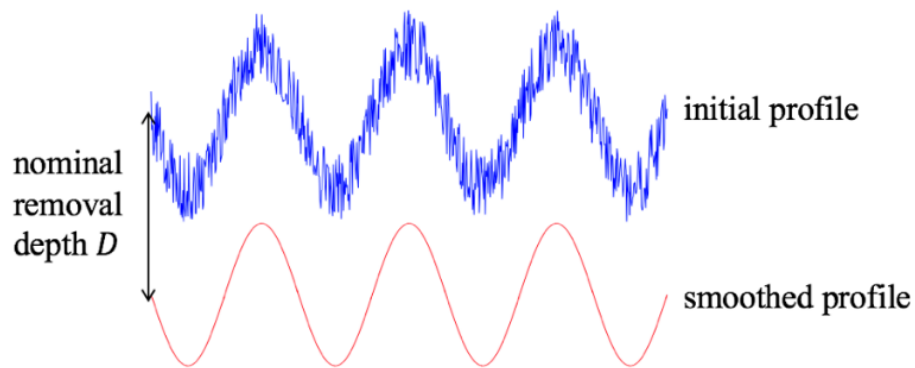


Figure 5 Ideal post-processing using PROS process, which removes a uniform layer of materials (i.e., nominal removal depth) while maintaining the original surface profile and improves the high spatial frequency surface finish.

3.1 Preston's Equation

The material removal process during optical fabrication is described by Preston's equation²³ as

$$\Delta z(x, y) = \kappa \cdot P(x, y) \cdot V(x, y) \cdot \Delta t(x, y), \quad (1)$$

where x and y are local coordinates on the workpiece surface, $\Delta z(x, y)$ is the integrated material removed, κ is Preston's constant defining the removal rate, $P(x, y)$ is the local polishing pressure, $V(x, y)$ represents the relative speed between polishing tool and workpiece, and $\Delta t(x, y)$ is the dwell time of the polishing tool.²⁴

Conventional polishing often proceeds by “charging” a compliant lap with polishing slurry and rubbing it against the surface of the optic. Solid particles in the slurry adhere to the tool and slide (not roll) against the surface.²⁵ The interface materials like the lap and slurry are important aspects governing Preston’s constant. Thus, to achieve a uniform removal depth D in PROS CNC post-processing, critical factors are maintaining a stable slurry application, uniform distribution of polishing pressure, and random distribution of the velocity vectors (speed and direction) along the smoothing path between the tool and optical surface.

3.2 PROS Post-Processing Interface Material

3.2.1 Post-Processing Lap/Tool

The polishing lap usually consists of a compliant layer, typically, of pitch or pad on a stiff substrate.¹³ In this case, aluminum or brass plates with a center joint hole are chosen as the base substrate. The tool size is selected to be the same as the size of the workpiece.

Pitch is a material derived from tree resin, usually dark color.²⁵ Polymer-based synthetic versions are also available.²⁶ For centuries pitch laps have been used to polish optics, two of the most important properties of a pitch is viscosity, and the ability to embeds polishing compounds. The viscosity is related to the ability to take on a desired form (flat, spherical, aspherical) and to slightly alter or adjust the form of the lap during polishing.²⁷ Gugolz pitch from Switzerland is widely used and Table 1 presents the specification data of the commonly used Gugolz pitch.

Table 1 Gugolz polishing pitch technical data.²⁸

Model	Specifications	Melting point (°C)	Softening point (°C)	Working Temperature (°C)
Gugolz #55	Very soft	72	63-64	15.5-18
Gugolz #64	Soft	68-72	65-68	18-24
Gugolz #73	Medium	77-80	71-74	24-32
Gugolz #82	Hard	79-82	75-77	Above 32

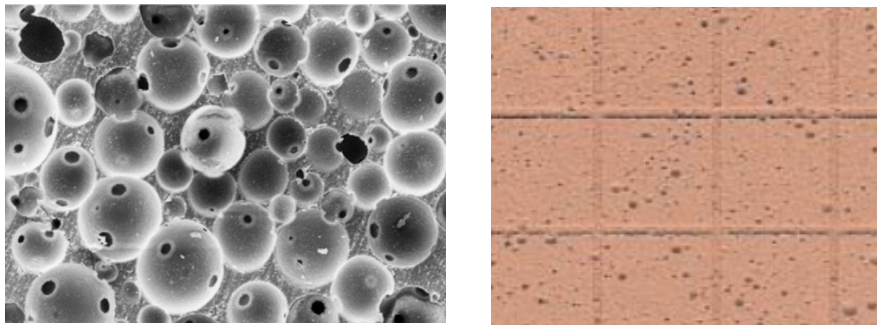
To achieve better matching and proper hardness of the pitch lap tool, we use the combination of #64 and #73 pitches shown in Figure 6.

**Figure 6** Gugolz #63 and #73 pitch.

Polishing pads are also commonly used for the polishing process. Compared to the pitch, pads are easier to affix to a backer and more consistent (i.e., requiring less maintenance). Also, they offer a variety of surface textures.¹³ For instance, Polyurethane pads like the cerium oxide-filled LP-66 is the most popular one. We applied this kind of pads to the PROS post-processing on PMMA optics. The specific properties are shown in Table 2 and the pad surface texture and the microphotograph by scanning electron microscope (SEM) are presented in Figure 7.

Table 2 LP-66 polishing pad properties.²⁹

Filler	Density (g/cm ³)	Hardness (Shore A)	Compressibility (%)	Elastic rebound (%)
Cerium oxide	0.42	80	9.4	84

**Figure 7** SEM microphotograph (left) and texture (right) of LP-66 polishing pad²⁹

For soft material polishing, like aluminum, napped pads are widely used. Napped pad could be fiber or engineered porometric. It has thin free-standing stalks on their surface that act like a brush to soften contact.¹³ We use the Black CHEM2 pad shown in Figure 8 (from PACE Technologies) for Al6061 post-processing experiments in the later discussion. This is a porometric polymer napped pad with consistency and is similar to a rubber-type pad. It behaves as an intermediate polishing pad, showing performance between those of low-napped and high-napped pads.³⁰

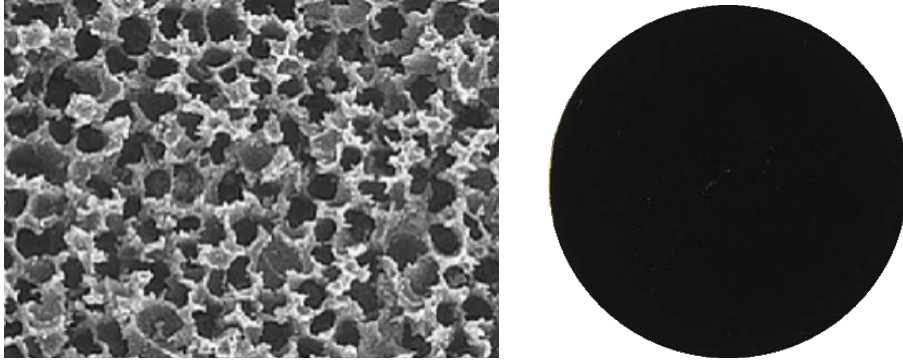


Figure 8 SEM microphotograph (left) and texture (right) of Black CHEM2 polishing pad.³⁰

The shape of the PROS post-processing lap must take the exact form of the desired optic. Otherwise, the optical surface profile will be changed.¹² Avoid that situation, whether we use pad or not, the pitch tool is made, and the pad is adhered to the pitch lap. Melted pitch is poured onto a rigid base and pressed against the sample reference shape. The pressing process is depicted in Figure 9.

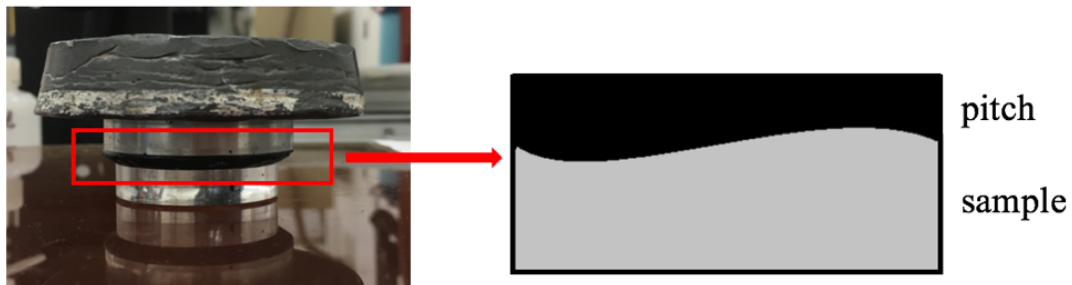


Figure 9 Pitch tool pressing process.

If the pitch lap without pads works as the PROS post-processing tool, as the pitch cools a razor is used to insert channels as shown in Figure 10. The channels allow the slurry to be evenly distributed and give the space for pitch to flow.



Figure 10 Pitch lap with channels.

3.2.2 Polishing Compound and Slurry

The slurry consists of abrasive particles (polishing compound), typically of ceria (for glass) or alumina (for metals and crystals), fluid carrier (solution), and optional additives like lubricants, detergents and so on.¹³

Cerium oxide (CeO_2 , ceria)¹³ has been the most widely used compound for glass in the last half century, whether pure or in combination with other rare earth materials. It is softer than most glass and friable (easily crumbled). It is available in premixed suspensions or dry powder form. Particle size for various grades range from 0.3 to 3.0 μm . CeO_2 is usually suspended in water and has a natural pH of around 8, but it has been used at various pH values from pH 4 to pH 9.5. Also, Zirconium oxide (ZrO_2 , zirconia) can be a substitute for CeO_2 for certain applications.

Rhodite 906 (in Figure 11) is a widely used cerium based polishing compound, and we apply this material to the PROS post-processing of BK7 and PMMA optics. The corresponding technical data is provided in Table 3. Rare Earth Oxide is a mixture of Cerium Oxide, Lanthanum Oxide, Praseodymium Oxide, and Neodymium Oxide. The rare

Earth Fluoride is a mixture of Cerium Fluoride and Lanthanum Fluoride.³¹ We choose water as the solution and the ratio between the compound and solution is about 1:3.

Table 3 Rhodite 906 technical data.³¹

Color	Average particle size (μm)	pH	Component	Weight (%)
Brown	1.8	6.5	Rare Earth Oxide	60-70
			Rare Earth Fluoride	30-40



Figure 11 Rhodite 906 polishing powder.³²

Aluminum oxide (Al_2O_3 , alumina)¹³ is used primarily for crystals, metals, semiconductors, and plastics. With a flat platelet shape and narrow size distribution, Al_2O_3 produces high-quality surfaces. It most commonly comes in dry powder form and requires a suspension agent to prevent caking.

Linde abrasive is a kind of alumina, with the properties supplemented by an extremely uniform control of particle size within a narrow range at the sub-micron level. Because of its ability to successfully finish a broad range of materials, including ceramics,

ferrites, ferrous and non-ferrous metals, composites, plastics, and glass, it has been used as a classic metallographic finishing media. It is readily compatible with cloth and synthetic material laps and provides a simple low-cost polishing procedure.³² For the post-processing on Al6061, we use the Linde B alumina compound (in Figure 12) specified in the technical data in Table 4.

Table 4 Linde B technical data.³³

Color	Average powder size (μm)	pH	Component	Weight (%)
white	0.05	-	Aluminum Oxide	99.9



Figure 12 Linde B alumina compound.³³

Finally, we choose olive oil as the solution and the ratio between the compound and solution is about 1:5. Detailed information for PROS post-processing for each sample application are discussed in Section 5.

3.3 Small Stroke CNC Pseudo-random Orbiting Stroke

It is difficult to adapt the asymmetric surface shape and matching of the tool and optics with large stroke motion, especially for smoothing freeform optics. Thus, we apply the small orbital stroke motion for the post-processing process, allowing pitch flow and continuous conforming to the shape³⁴ simultaneously.

The regular tool path will contribute to the systematic misfit between the tool and workpiece, which will lead to directionality of the surface profile in the final product. Even with small stroke motion, a smooth path with directionality is impossible to maintain in the original surface profile. A full-aperture small stroke directional experiment on an SPDT PMMA material is implemented to experimentally prove and confirm the undesired directional characteristic in the surface profile. The tool stroke pattern follows a 2 mm horizontal (x direction) linear motion, and the surface freeform pattern for the SPDT surface is spiral. The top view of the experiment setup as well as the smoothing parameters are described in Figure 13, where d stands for the stroke distance.

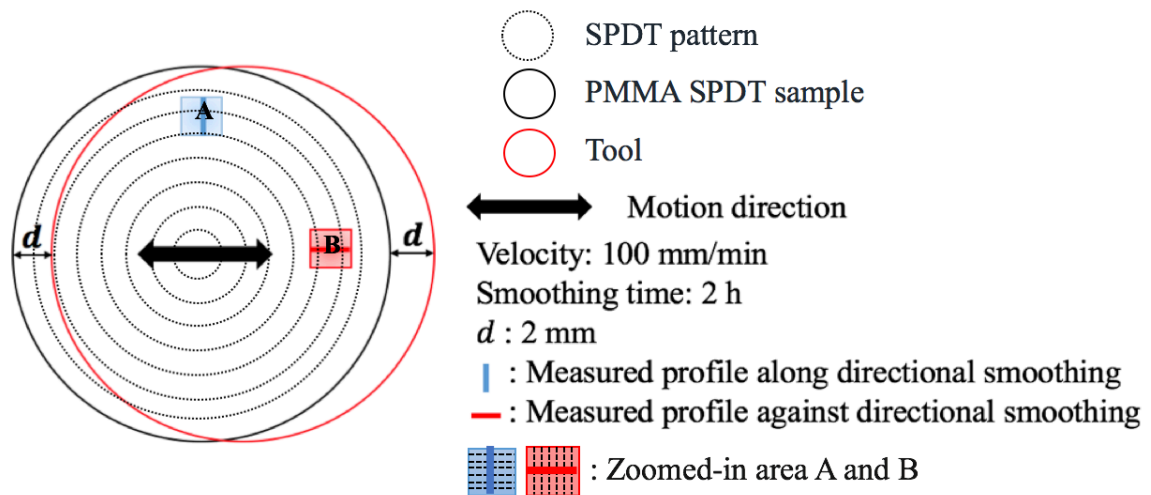


Figure 13 Top view of the directional experiment setup.

We compare the smoothing effect in two profiles (shown in Figure 13) of this PMMA sample. The first concerns the smoothing direction against the diamond-turned pattern, and the second, along the diamond-turned pattern. The direct measured initial and smoothed surface profiles as well as power spectral density (PSD) comparison for each smoothing process are shown in Figure 14.

The PSD can represent the scattering properties. Here, it's related to the tool mark left by the SPDT process. Quantitatively, the PSD represents the spatial-frequency spectrum of the surface roughness measured in inverse-length units. Roughness values are obtained from the area under a band-limited part of the PSD function. The one dimensional 1-D PSD is the square of the Fourier transform of a linear surface profile.³⁵

Assuming 1-D profile with the surface roughness height $h(x)$ as a function of distance x ($0 < x < L$) and L as the profile length, the Fourier transform of the finite measured length can be written as:

$$H(k) = \int_0^L h(x) \exp(-ikx) dx, \quad (2)$$

and the PSD can be expressed as:

$$\text{PSD} = \left\{ \frac{|H(k)|^2}{L} \right\}, \quad (3)^{36}$$

where k is the wavenumber.

The measured profile data of the experiments is provided by NewView™ 8000 white light interferometer (ZYGO). By setting the measurement location on the control software, it will compare the line profiles at nearly the same location. Using the PSD analysis function, it offers the PSD value across the measured dimension shown in Figure 14.

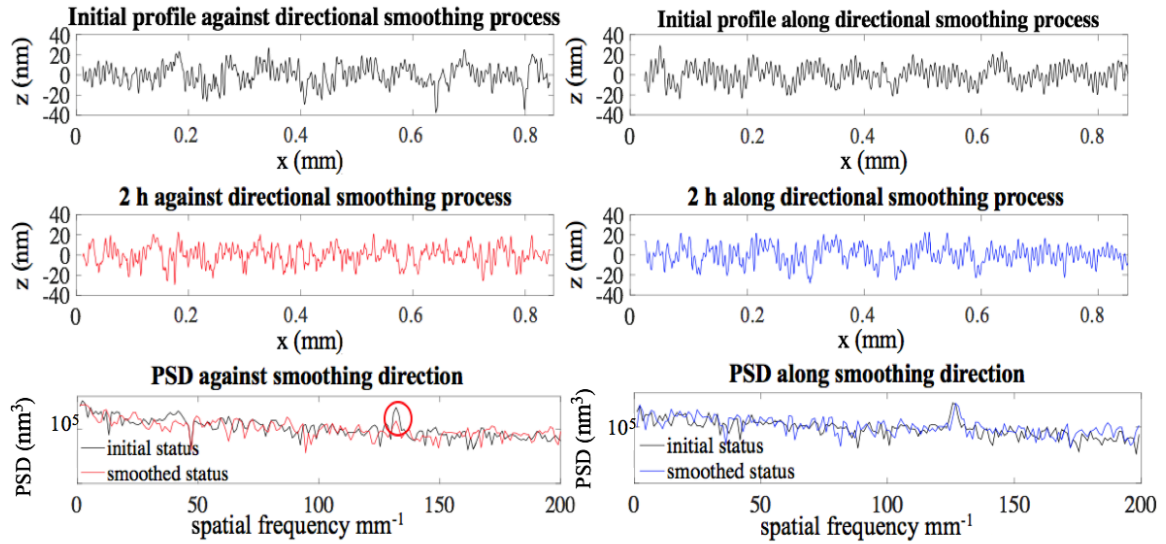


Figure 14 Surface profile comparison: PSD against (left) and along (right) directional smoothing process.

The corresponding micro-surface roughness value and varied ratio of the initial and smoothed states are presented in Table 5. Note that the against smoothing direction result shows that the roughness parameters peak-to-valley (PV) and average roughness (Ra) decrease by about 20% and 10%, and the PSD for the high spatial frequency improves, which presents in the red circled area in figure 4. However, the along smoothing direction result does not show much variation. Therefore, the smoothing direction affects the smoothing result considerably. The high spatial frequency errors can only be removed if the smoothing direction is always opposite to the direction of error. Thus, in order to achieve global smoothing effect, the direction of the smoothing process should be randomly distributed in every direction.

Table 5 Roughness parameters PV and Ra for each surface profile in each smoothing process.

	Measured profile direction in Fig. 14	Initial state	Smoothed state	Varied ratio
PV (nm)	Against (red line)	64.82	51.88	19.96%
Ra (nm)		8.10	7.20	11.11%
PV (nm)	Along (blue line)	53.61	50.97	4.92%
Ra (nm)		7.47	7.50	0.4%

Accordingly, we set our smoothing path as a PROS pattern, in which the ending position coincides with the beginning position. To operate such a smoothing path, G-Code language is applied and a MATLAB-based data processing module was developed. As the pin connects the center of the tool and the CNC machine, the position of the smoothing path is related to the tool's center position.

The initial position of the PROS path is defined by the parameter named "offset" (mm) in this module. The initial offsets for x and y are usually 0, which means that the center of the tool coincides with the center of the workpiece. We use the polar coordinate system for setting up the parameters for the orbital stroke. The largest orbital radius of each stroke of the PROS tool path is defined as r_{max} . To achieve uniform removal depth, during the PROS process, each stroke radius is randomly selected within the value of r_{max} . At the same time, the angle of each PROS circular path is randomly distributed in order to ensure the pseudo random characteristic of the stroke. The velocity is also randomly distributed within the range of the given maximum feed rate (mm/min). The uniform random distribution is used in the PROS path generation.

The running time (min) in the module roughly defines how many circular patterns will exist during the whole smoothing process.

Figure 15 shows the relationship among maximum radius r_{max} , Pseudo-random orbiting stroke tool path, as well as the smoothing area. The black, red, and blue circles represent the tool, workpiece, and tool path respectively. The red o denotes the beginning position. c_1 and c_2 are two example positions of the tool center during the PROS post-processing with radius r_{max} , and the blue shaded area is the uniform smoothing area or the area where the tool always contacts the workpiece.

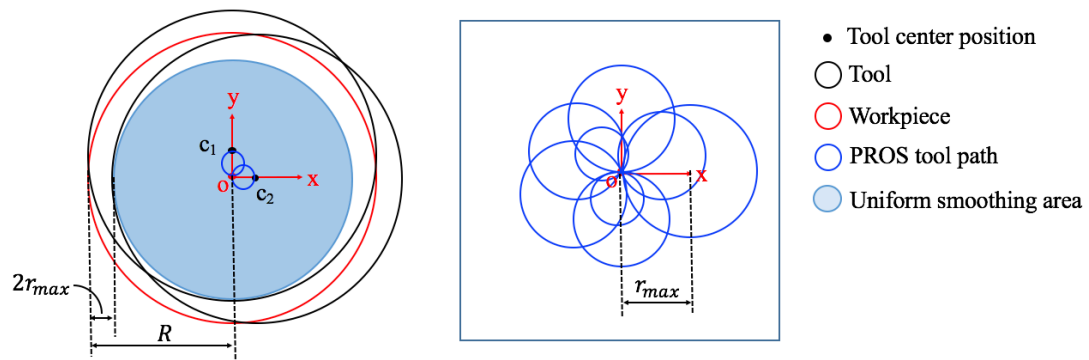


Figure 15 Schematic showing the geometrical relationship between the workpiece and tool (left) and the PROS tool path generated using the CNC machine control software (right).

When the sizes of the tool and workpiece are the same, the uniform smoothing area cannot cover the whole workpiece. We set the radius of workpiece as R , so that the ratio between the uniform smoothed area and the workpiece area E is

$$E = \frac{(R-2r_{max})^2}{R^2} \times 100 \%. \quad (4)$$

The workpiece size or smoothed area is the uniform smoothed area, and the measured diameter in the presented work corresponds to the effective diameter.

In summary, the goal of PROS post-processing technique is explained at the beginning of this Section. Followed by the Preston's equation, various fabrication materials

are described in detail. This Section also provides key features on the PROS post-processing technique, which are shown in table 6.

Table 6 Key features in PROS post-processing technique.

Parameters	Description
Post-processing tool	Full aperture
Stroke direction	Randomly assigned
Stroke radius (mm)	Maximum orbital stroke radius r_{max} assigned Each stroke radius is randomly selected within the value of r_{max}
Feed rate (mm/min)	Maximum feed rate (mm/min) assigned Velocity is randomly distributed within the range of the feed rate.
Pressure (psi)	Uniform

The pseudo-random orbital stroke tool path is discussed and the directional smoothing experiment case is studied to justify the necessity for the PROS tool path. The PROS process hardware and control software discussions are presented in Section 4.

4 CNC PROS MACHINE AND SOFTWARE

The CNC machine used for the PROS optical smoothing process is a 4-Axis CNC Router (ONLY 3 axis are used for the PROS post-processing technique), named as “24W-ACE”. This is purchased from Velox CNC as an upgraded CNC Router. Mach 3 CNC software is used for running the G-code produced by the stroking software. Basic specification data of the Velox CNC machine is provided in Table 6.

Table 7 machine specification.³⁷

Specifications	x	y	z	units
Machine travel	24	24	8	inch
Leadscrew diameter	5/8	5/8	1/2	inch
Travel per turn	1/4	1/4	1/5	inch
Maximum travel per turn	200	200	150	inch / min
Stepper motors	600	600	280	oz / inch
Rapid speeds	100	100	100	inch / min
Resolution	0.00035	0.00035	0.00025	inch
Repeatability (+/-)	0.001	0.001	0.001	inch
Overall foot print	42''x42''x34''			
Drive mechanism	Acme leadscrew and anti-backlash nut			
Weight	175 lbs			
Control box	3-Axis smooth step ethernet control box			
Control software	Mach 3 control soft ware			
Home switches	Installed on all axes			

4.1 CNC Machine Configuration

To perform the pseudo random orbital stroke, the X and Y axes allow for a repeatable orbital motion. The additional Z axes is required for aligning the tool to the work piece safely. The Z motion allows for various work pieces and tools to be attached to the machine, giving the User more freedom in choosing experiments. We do not use the A axis, which is also known as the Spin axis, to control the rotation. But the Spin axis is controllable via g-code and could be used in the future for stroking operations.³⁸

The PROS CNC Setup is presented in Figure 16. The workpiece is fixed by two clamps and one fixed screw along the circumferential direction. The tool is driven by a pin to provide the degree of freedom for linear motion in the x and y directions as well as rotating motion, and lubricant is added to the connection area to ensure free rotation. Pressure is loaded by attaching an extra uniform weight. The centers of both the tool and workpiece coincide at the beginning and finishing points.

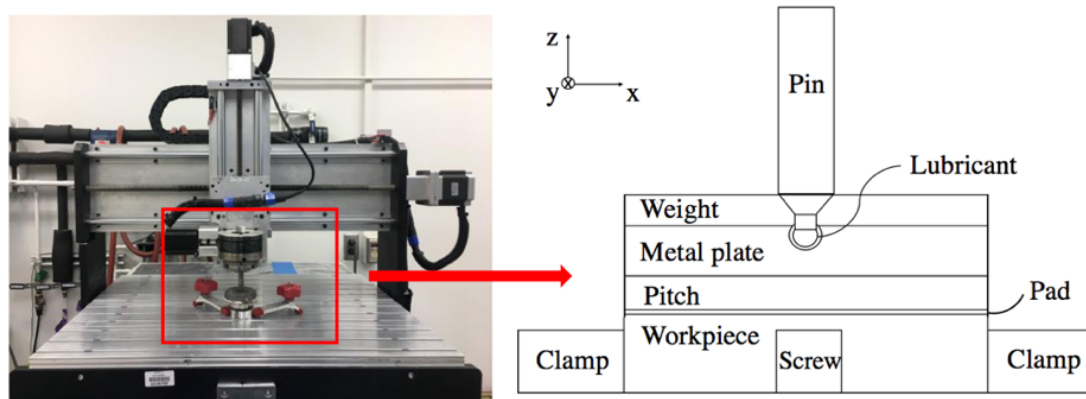


Figure 16 Schematic of the PROS process CNC setup.

4.2 Mach 3 Software and G Code

The Velox CNC Stroking Machine's Control Computer came preinstalled with Mach 3 and it is preconfigured to function as a CNC Mill. The Mach 3 software interfaces with the Windows Kernel to ensure that the CNC is performing at a specified update rate. Figure 17 shows the user-interface of the software.

The left-up green panel with a vertical scroll bar indicates the lines of G code that are presently loaded into the software. The controls below allow the operator to Load G Code, Edit G Code, Cycle Start, Stop, and Reset. The next set of controls is in the top center region of the screen. These controls control the motion of the 4-Axes and the ability to zero their encoders. Next, the machine may be positioned by using the keyboard arrow keys for

X and Y axes movement while the Page Up / Page Down keys control the Z axis movement.³⁸

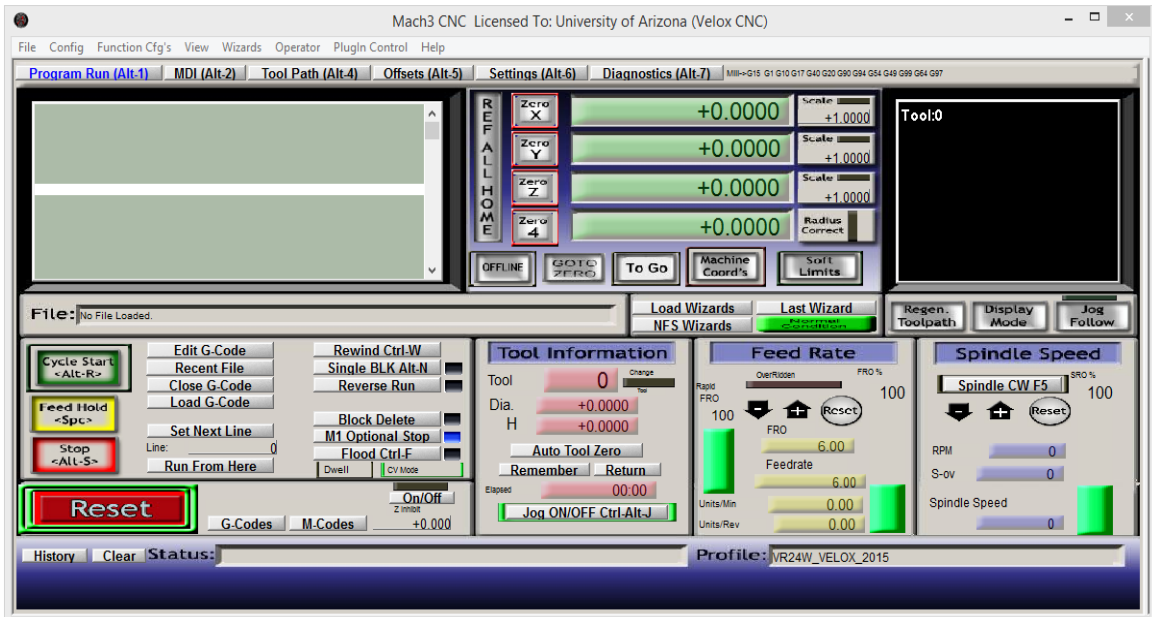


Figure 17 User-interface of Mach 3 control software.³⁸

The G Code language³⁹ was created by machinists to control the motion of Computer Numerically Controlled (CNC) machines, and it is largely standardized language in the machining industry. The language itself consists of a one letter command followed by a numeric command code. It is through many codes and sequences that define machine parameters: units (mm or inches), feedrate (mm / min, inches / min, revolutions / min), absolute position mode or incremental position mode, plane select, etc. Table 7 presents several G Code examples.

Table 8 G Code examples.³⁹

G Code	Command
G00	Rapid move
G01	Linear feed move
G02	Clockwise arc feed move
G03	Counter clockwise arc feed move
G12	Clockwise circle interpolation
G13	Counter clockwise circle interpolation

5 EXPERIMENTAL SETUP AND METROLOGY CONFIGURATION

5.1 PROS Post-processing Experiment Setup

Three representative experimental cases are discussed in this section, each with a different optics material, pre-polishing method, and surface shape. The initial-state descriptions of all workpieces are listed in Table 8, and the basic post-processing information appears in Table 9.

Table 9 Description of the initial states of the BK7, PMMA, and Al6061 workpieces.

	BK7	PMMA	Al6061
Pre-polishing method	MRF	SPDT	SPDT
Freeform profile	Spiral	Trefoil	Astigmatism
Diameter (mm)	100	30	50.8
Effective diameter (mm)	96.4	28	44
Radius of curvature (mm)	136.8	120	∞
Central obscuration ratio	0.2	0	0.33

As listed in Table 9, the post-processing tool for workpiece BK7 is a pitch tool, and pads are chosen and joined to the pitch tool for PMMA and Al6061. LP-66 is a cerium oxide-filled polyurethane pad and the black CHEM2 pad is a porometric polymer pad with consistency similar to a rubber-type pad. It behaves as an intermediate polishing pad, showing performance between those of low-napped and high-napped pads.¹³ Unlike the post-processing for the BK7 and PMMA samples, two stages exist in the case of the Al6061 sample. The first stage lasts 600 min with 50 nm alumina compound mixed with olive oil, and the second stage lasts 90 min with pure olive oil. The total running time was decided by observing the saturation (i.e., no more improvement) of micro-surface roughness for each sample.

Table 10 Post-processing information of the BK7, PMMA and Al6061 workpieces.

	BK7	PMMA	Al6061
Maximum feed rate (mm/min)	100	100	100
Maximum radius r_{max} (mm)	1	1	1
Pressure (psi)	0.3	0.3	0.1
Pitch type	Combination of #64 pitch and #73 pitch (common)		
Pad type	-	LP-66 pad	Black CHEM2 pad
Solution	Water	Water	Olive oil
Post-processing compound	Rhodite 906	Rhodite 906	S1: 50 nm Alumina S2: -
Running time (min)	40	105	S1: 600 S2: 90

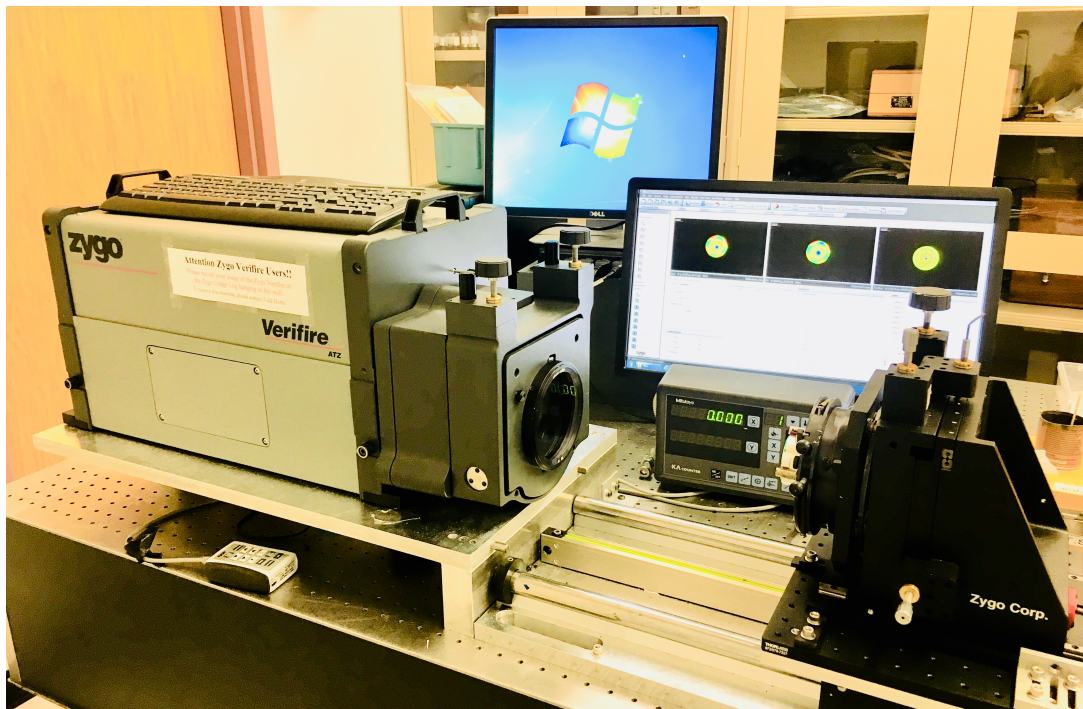
5.2 Measurement Configuration for Data Acquisition

A VeriFireTM interferometer (ZYGO)⁴⁰ is used to analyze the full aperture surface map. The results of directly measured initial and smoothed surface maps will support the maintenance of the surface profile.

The VeriFireTM interferometer is an industrial grade high power Fizeau interferometer with patented QPSITM acquisition for true on-axis common path surface form metrology in the presence of vibration. This instrument can measure surface from of reflective materials and optics, the transmitted wavefront of transparent optics and imaging system. Specification data sheet offered by ZYGO company is in Table 10. Figure 18 is the actual instrument used for the experiments in the lab.

Table 11 Specification data of the ZYGO VeriFire™ interferometer.⁴⁰

Test beam diameter	Alignment FOV	Camera details		Laser source	Performance	
4 inch (102 mm)	± 3 degrees	Resolution	1200 × 1200 pixels	High power stabilized HeNe	RMS simple repeatability	< 0.06 nm
		Frame rate	160 Hz		Wavelength: 633 nm	RMS wavefront repeatability
		Digitization	8 bit		Peak pixel deviation	< 0.5 nm

**Figure 18** VeriFire™ interferometer used for the PROS process experiments.

White-light interferometry has recently become a well-established method in microscopic profilometry.³⁶ A NewView™ 8000 white light interferometer (ZYGO) is used to analyze the micro-surface roughness condition, and we choose Ra, the arithmetical mean deviation, to present the results.

The same square-shaped location measurement pattern is set for the whole surface. The micro-surface roughness result of each smoothing phase is given by the average Ra value of all measurements. Table 11 describes the measurement setup parameters and measurement patterns for three experiments.

Table 12 Measurement patterns for three experiments.

	BK7	PMMA	Al6061
Pattern area (mm ²)	64	25	36
Point spacing (mm)	1	0.625	0.75
Number of sampling points	9 × 9	9 × 9	9 × 9

The measurement technique in NewView™ 8000 white light interferometer (ZYGO)⁴¹ is 3D coherence scanning interferometry and phase shifting interferometry. The precision Piezo drive with closed loop capacitance gauge control and crash protection are applied to the scanner. Table 12 is the specification data offered by ZYGO company. Figure 19 is the actual white light interferometer instrument used for the PROS process experiments in the lab.

Table 13 Specification data of the NewView 8000 white light interferometer.⁴¹

Specification	Value
Vertical scan range	0.15 - 20 mm
Surface topography repeatability	0.2 nm
Repeatability of RMS	0.01 nm
Optical lateral resolution	0.34 micron under 100× objective lens
Maximum data scan speed	96 μ/sec

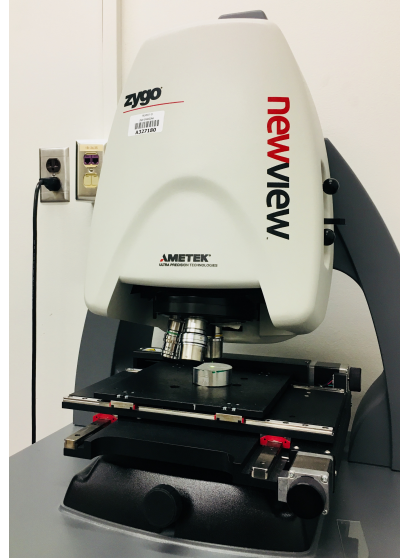


Figure 19 NewView white light interferometer used for the PROS process experiments in the lab.

The PROS post-processing measurement parameter settings for white light interferometer are listed in Table 13.

Table 14 Measurement setup parameters for the white light interferometer.

Measurement Setup	Settings
Objective lens	10× Mirau NA 0.3
FOV (mm)	0.83 × 0.83
Lateral resolution (micron)	0.815
Number of times measurements were taken to obtain an average	3

In summary, this Section focus on the experimental setup and metrology configuration. The specification data on each optics sample, post-processing process are provided. The metrology instruments (VeriFireTM interferometer and NewViewTM 8000 white light interferometer) used for the full aperture surface form maintenance check and the micro-surface roughness measurements are introduced.

6 FREEFORM OPTICS POST-PROCESSING PERFORMANCE

The post-processing time and final surface quality are determined by the material characteristics and initial surface quality. Notably, the final smoothed state of all the experiment samples showed good full aperture surface freeform maintenance as well as improvement in surface quality.

6.1 Surface Form Preservation Analysis

Figure 20 presents the measured initial and smoothed maps as well as the subtracted maps for each workpiece. Tables 8 provides more details of the sample surfaces including the effective diameters for each case.

The maps in the initial stage are almost the same as those in the smoothed stage. Focusing on the subtracted map, which indicates the criterion for full aperture freeform surface maintenance, the full aperture root mean square (RMS) value is about 0.05λ (assuming $\lambda = 633 \text{ nm}$), and the varied ratio of the initial and smoothed states is within 5%. The corresponding full aperture PV and RMS comparisons are summarized in Table 14.

Table 15 Full aperture PV and RMS comparisons of the initial, smoothed, and subtracted maps for BK7, PMMA and Al6061.

Parameters	Materials	Initial map	Smoothed map	Subtracted map	Varied ratio
PV (nm)	BK7	3216.32	3125.76	442.05	13.74%
RMS (nm)		804.76	801.16	33.65	4.18%
PV (nm)	PMMA	2552.23	2196.70	298.55	11.69%
RMS (nm)		481.74	421.68	23.99	4.98%
PV (nm)	Al6061	1838.43	1794.04	266.54	14.47%
RMS (nm)		276.54	250.54	13.52	4.89%

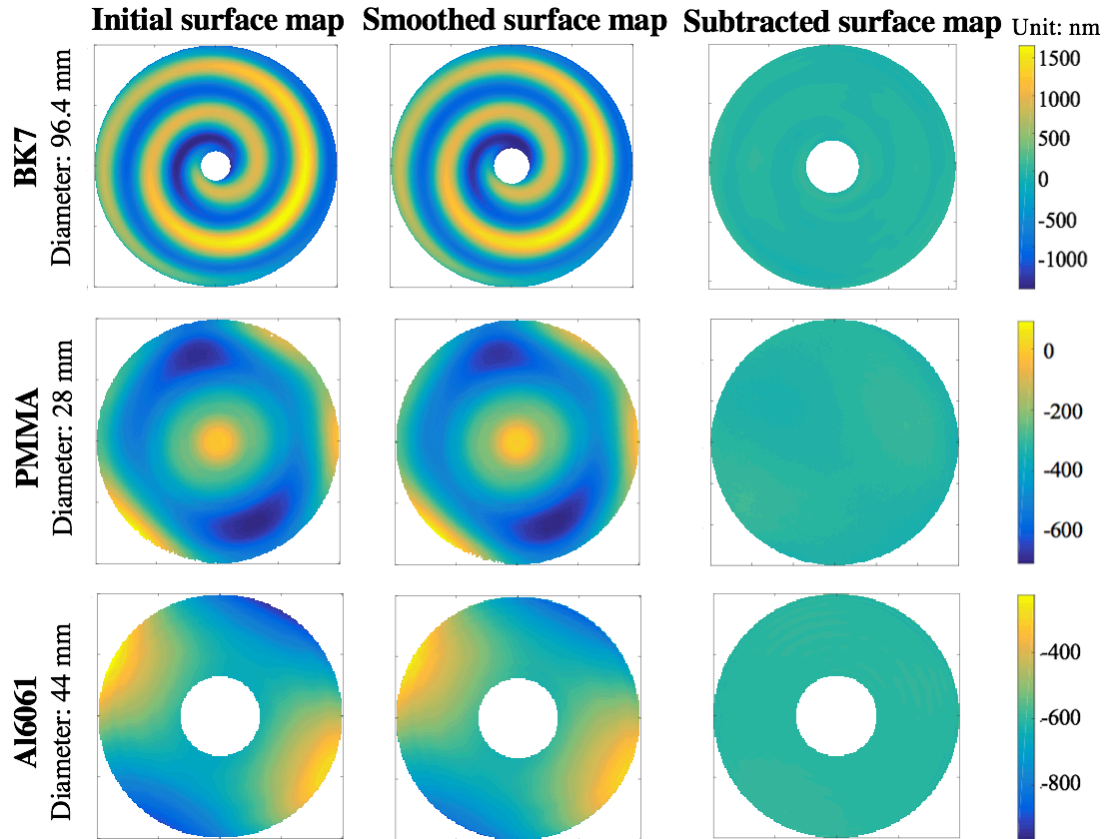


Figure 20 Measured full aperture maps using VeriFire™ interferometer for the initial and smoothed stages, and the corresponding subtracted surface map showing the difference between the before and after the PROS process.

6.2 Analysis of Micro-Surface Roughness Improvement

After the post-processing, an improvement in the micro-surface roughness is evident for all workpieces, as illustrated in Figure 21. The smoothing times for the intermediate and final states for each sample are provided in Table 15.

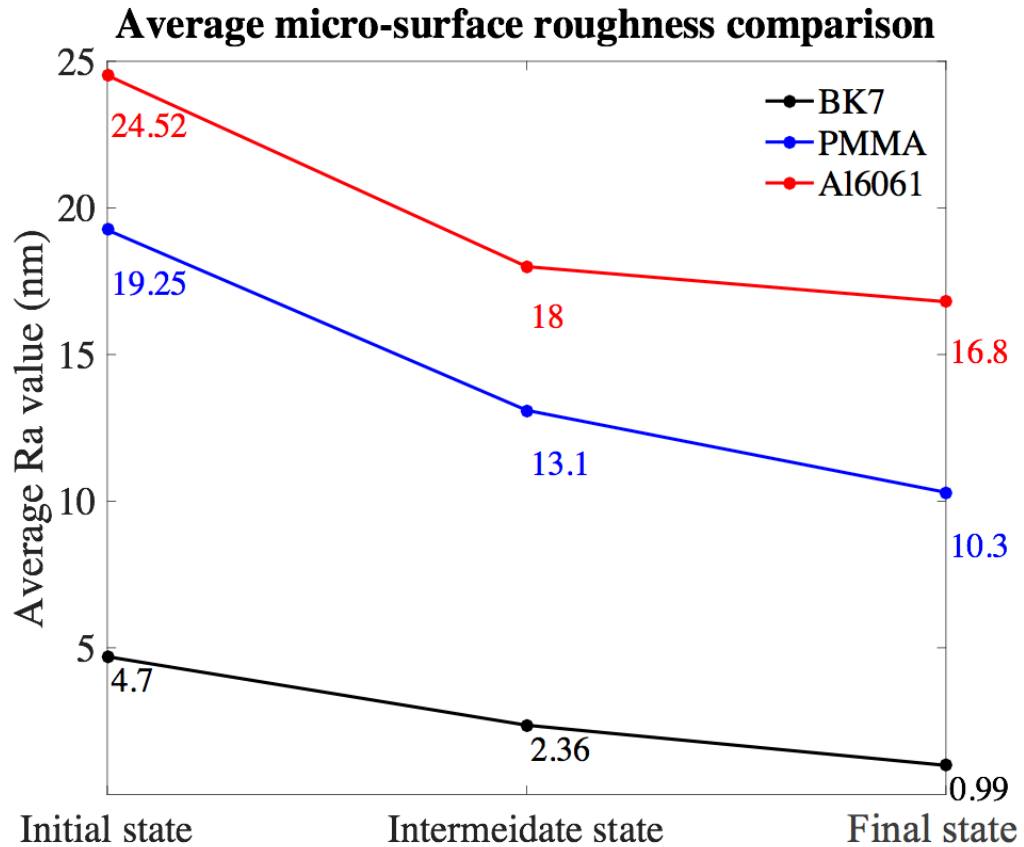


Figure 21 Micro-surface roughness comparison of all samples.

The micro-surface roughness decreases with post-processing time, and the decreased ratios from the initial to the final state for BK7, PMMA, and Al6061 are 78.93%, 46.49%, and 31.48%, respectively. The post-processing value depends on the original surface quality.

Table 16 Smoothing times for each stage for BK7, PMMA, and Al6061.

	BK7	PMMA	Al6061
Intermediate state	10 min	45 min	540 min
Final state	40 min	105 min	690 min

Moreover, a change in the statistical micro-surface roughness (Ra) distribution is observed when tracking the result of each measured sampling point. We set the histogram Ra binning range as 1 nm. Figure 22 describes the statistical distribution of measured micro-surface roughness (Ra) as the PROS post-processing is applied.

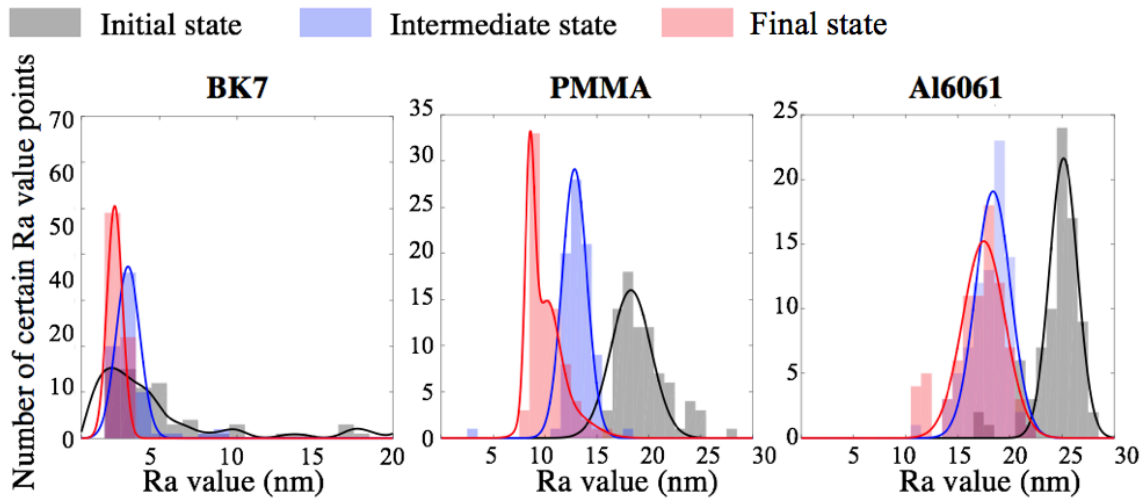


Figure 22 Distribution of measured micro-surface roughness (Ra) against various states. The bars and curves stand for the micro-surface roughness distribution and fitted curve in each state, respectively.

The initial distribution state depends on the previous polishing methods (e.g. MRF and SPDT). For each final smoothed state, the Ra value increases and the peak value of the fitted curve moves to the left smaller Ra values as a result.

On a microscopic scale, the improvement in surface roughness and high spatial frequency errors are obvious. Considering that BK7 is polished using MRF, and the high spatial frequency errors are well-controlled, we focus this discussion on the SPDT PMMA and Al6061 workpieces. Comparing the same measured areas, the tool marks from SPDT gradually disappear. Choosing a line across the diamond-turned pattern of the surface map and analyzing the PSD as seen in Figure 23, we note that the high spatial frequency errors are eliminated as a result of the PROS process.

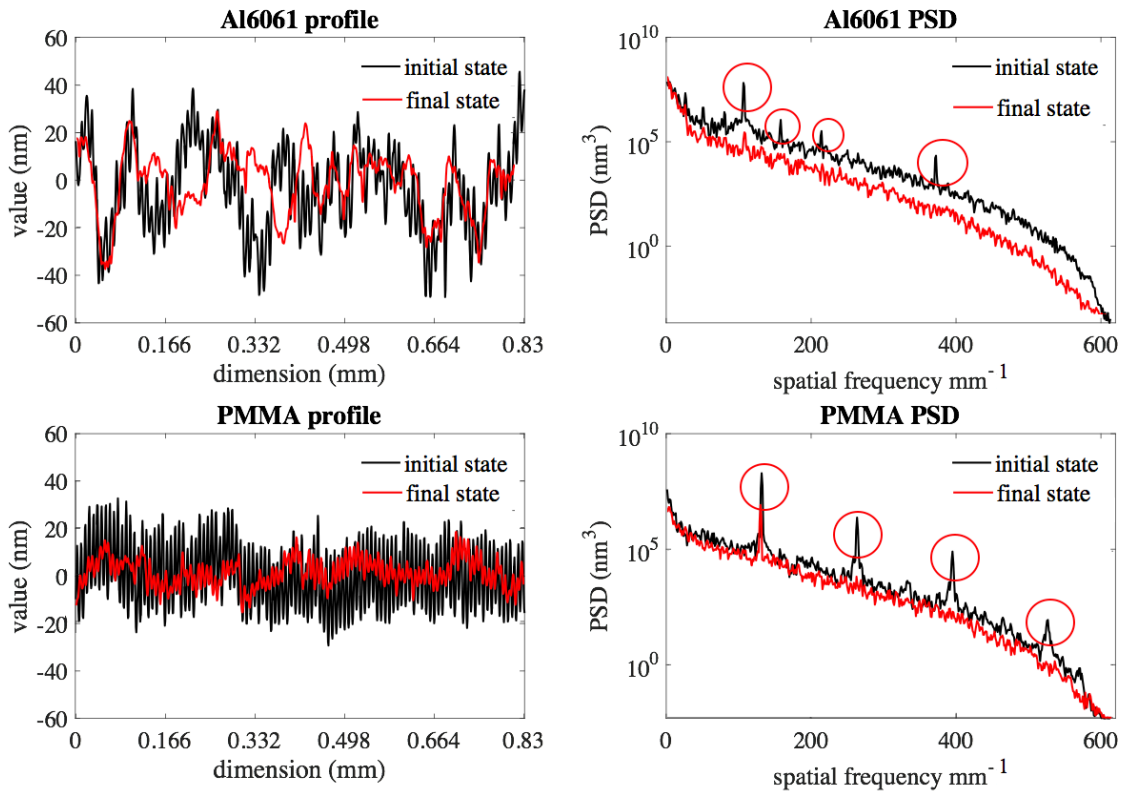


Figure 23 Analyses of linear profile data (left) and PSD (right) for the SPDT PMMA and Al6061 samples before and after the PROS post-processing.

The circled peak in the initial state is successfully eliminated in the final smoothed state, and thus, the single measurement profiles are smoother after the PROS post-processing. The clear suppression of the diffraction phenomenon from the previous SPDT process can also be observed visually. An example of the Al6061 workpiece is presented in Figure 24.



Figure 24 Visual appearance of the Al6061 sample before (left) and after (right) the smoothing process.

The figure on the left shows the sample before the smoothing process. The reflected image is clear and a significant diffraction phenomenon exists, which is caused by the periodic tool marks. The figure to the right is the smoothed sample, and we note that the diffraction phenomenon disappears and the reflected image is clearer meaning less scattering and diffraction.

Thus, we can conclude that the PROS CNC-based post-processing technique can maintain full aperture profiles for freeform optics while improving the surface quality; the finished samples exhibit lower micro-surface roughness and fewer tool marks.

7 CONCLUSION

Modern freeform optics manufacturing is usually based on deterministic subaperture methods, and even though the desired surface form can be achieved, higher micro-surface roughness and fewer high spatial frequency errors still pose barriers to a successful manufacturing process. The PROS CNC-based post-processing technique presented in this paper is able to maintain the original correct surface form while improving small-scale surface quality, and thus, it provides a convenient solution in freeform optics for different materials and apertures.

Three detailed independent experiments using different workpieces and finishing techniques, namely, BK7 (MRF), PMMA (SPDT), and Al6061 (SPDT), with distinctive surfaces are presented in this paper. Choices for slurries and parameter setup during the post-processing are also listed and specified in details to provide authors a re-traceability of the presented experimental data, which is very critical information as a fabrication research report. The varied ratio of the initial and final smoothed states in the full aperture map is within 5% for all three cases. These measured results prove the robust maintenance of the surface initial forms. Our tracking of the micro-surface roughness in each post-processing state for all cases and the PSD analysis for the two SPDT workpieces demonstrated the improvement in surface quality when using the proposed technique.

REFERENCES

1. X. Guo, Y. Shu, G. Kim, M. Palmer, H. Choi, D. W. Kim “Pseudo-random orbiting stroke for freeform optics post-processing,” *Opt. Eng.*, SPIE (to be submitted).
2. R. A. Jones, “Grinding and polishing with small tools under computer control,” *Opt. Eng.* **18** (4), 184390 (1979). [doi:10.1117/12.7972392].
3. J. H. Burge, B. Anderson, S. Benjamin, M. Cho, K. Smith, and M. Valente, “Development of optimal grinding and polishing tools for aspheric surfaces,” *Proc. SPIE* **4451**, Optical Manufacturing and Testing IV (2001). [doi: 10.1117/12.453615].
4. T. T. Saito, “Diamond turning of optics: the past, the present and the exciting future,” *Opt. Eng.* **17**(6), 176570 (1978). [doi:10.1117/12.7972285].
5. D. W. Kim and J. H. Burge, “Rigid conformal polishing tool using non-linear visco-elastic effect,” *Opt. Express*. **18**(3), 2242–2257 (2010). [doi:10.1364/OE.18.002242].
6. D. D. Walker and C. R. Dunn, “Pseudo-random tool paths for CNC sub-aperture polishing and other applications,” *Opt. Express* **16**, 18942-18949 (2008). [doi: 10.1364/OE.16.018942].
7. H. Y. Tam, H. B. Cheng, and Z. C. Dong, “Peano-like paths for sub-aperture polishing of optical aspherical surfaces,” *Appl. Opt.* **52**(15), 3624–3636 (2013). [doi:10.1364/AO.52.003624].
8. I. Miyamoto, “Ultra fine finishing of diamond tools by ion beams,” *Precis. Eng.* **9**(2), (1987). [doi: 10.1016/0141-6359(87)90056-0].
9. J. D. Nelson, A. Gould, C. Klinger, and M. Mandina, “Incorporating VIBE into the precision optics manufacturing process,” *Proc. SPIE* **8126**, 812613 (2011). [doi: 10.1117/12.892735].
10. F. Z. Fang, X. D. Zhang, A. Weckenmann, G. X. Zhang, C. Evans, “Manufacturing and measurement of freeform optics,” *CIRP Annals - Manufacturing Technology* **63**(2), 541–556 (2013) . [doi: 10.1016/j.cirp.2013.05.003].

11. F. Z. Fang, V. C. Venkatesh, "Diamond Cutting of Silicon with Nanometric Finish," *CIRP Annals - Manufacturing Technology* **47**(1),45-49 (1998). [doi: 10.1016/ S0007-8506(07)2782-6].
12. T. Blalock, K. Medicus, J. D. Nelson, "Fabrication of freeform optics," *Proc. SPIE* **9575**, Optical Manufacturing and Testing XI, 95750H (2015). [doi: 10.1117/12.2188523].
13. Williams, R. (2011). *Field Guide to Optical Fabrication*. Bellingham, WA: SPIE.
14. H. M. Pollicove, "Innovations in deterministic optical manufacturing processes," *Proc. SPIE* **4921**, 16-19 (2002). [doi: 10.1117/12.481744].
15. H. N. Cheng, "specifying optics to be made by single point diamond turning", *OPTI 521 Tutorial Report*, https://wp.optics.arizona.edu/optomech/wpcontent/uploads/sites/53/2016/12/Tutorial_ChengHN.pdf. (2016).
16. M. C. Gerchman, "Specifications and manufacturing considerations of diamond-machined optical components" (PDF), *Optical Components Specifications for Laser-based Systems and other Modern Optical Systems* **607**: 36–45. (1986).
17. C. F. Cheung, W. B. Lee, "Modelling and simulation of surface topography in ultra-precision diamond turning," *Proceedings of the Institution of Mechanical Engineers*, **214**(6), 463 (2000).
18. Baumer, S. (2005). *Handbook of plastic optics*. Germany:Wiley-VCH.
19. J. D. Lytle, "Polymetric Optics", in *Handbook of Optics*, 2nd ed., edited by M. Bass (McGraw-Hill, New York, 1995), Chap. 34, Vol. II, p. 34.13.
20. J. Claracq, J. Sarrazin, Montfort, "Viscoelastic properties of magnetorheological fluids", *JP. Rheol Acta*, **43**: 38. (2004) [doi: 10.1007/s00397-003-0318-7].
21. K. Schwertz, "An introduction to the optics manufacturing", *OPTI 521 Tutorial Report*, https://wp.optics.arizona.edu/optomech/wpcontent/uploads/sites/53/2016/10/Katie_Introduction-to-the-Optics-Manufacturing-Process.pdf.
22. M. Tricard, P. Dumas, G. Forbes, "Subaperture approaches for asphere polishing and metrology," *Proc. SPIE* **5638**, Optical Design and Testing II, (2005). [doi: 10.1117/12.577539].

23. F. W. Preston, "The theory and design of plate glass polishing machines," *J. Soc. Glass Technol.* **11**, 214–256 (1927).
24. J. D. Hoyo, H. Choi, J. H. Burge, G. Kim, D. K. Kim, "Experimental to power spectral density analysis for mid- to-high-spatial frequency surface error control." *Appl. Opt.* **56**, 5258-5267 (2017). [doi: 10.1364/AO.56.005258].
25. N. J. Brown, "Optical polishing pitch," preprint of a paper prepared for submission to the Optical Society of America workshop on Optical Fabrication and Testing, (1977).
26. S. P. Sutton, "Development of new synthetic optical polishing pitches," *Frontiers in Optics, OSA Technical Digest (CD)* (Optical Society of America, 2004), paper OTuA2. [doi: 10.1364/OFT.2004.OTuA2].
27. B. E. Gillman, F. Tinker "Fun Facts about Pitch & the Pitfalls of Ignorance," *Proc. SPIE* **3782**, Optical Manufacturing and Testing III, (1999). [doi: 10.1117/12.369240].
28. Meller Optics, "Gugolz Polishing Pitch", <https://www.melleroptics.com/product-category/gugolz-polishing-pitch/>.
29. JHRHODES, "LP-66 PAD PROPERTIES (Average)," <http://jhrhodes.com/products/lp-66/>.
30. Pace Technologies, "Metallographic Polishing Pads (PSA)," <http://www.metallographic.com/Technical/Polishing-PSA.htm>. Accessed on 2006.
31. Universal Photonics, "Rhodite 906 Material Safety data sheet" <http://universalphotonics.com/Portals/0/MSDSs/rhodite906MS.pdf>.
32. F. R. Charvat, P. C. Warren, E. D. Albrecht, (1974). *Linde Alumina Abrasives for Metallographic Polishing*. In: McCall J.L., Mueller W.M. (eds) *Metallographic Specimen Preparation*. Springer, Boston, MA [doi:10.1007/978-1-4615-8708-8_6].
33. Universal Photonics, "Safety Data Sheet: Linde Alumina A, B, C" <http://universalphotonics.com/Portals/0/MSDSs/lindepowderMS.pdf>.

34. R. E. Wagner and R. R. Shannon, "Fabrication of aspherics using a mathematical model for material removal," *Appl. Opt.* **13**(7), 1683–1689 (1974). [doi: 10.1016/0895-7177(93)90056-5].
35. A. Duparré, J. F. Borrull, S. Gliech, G. Notni, J. Steinert, J. M. Bennett, "Surface characterization techniques for determining the root-mean-square roughness and power spectral densities of optical components," *Appl. Opt.* **41**, 154-171 (2002). [doi: 10.1364/AO.41.000154].
36. J. M. Elson and J. M. Bennett, "Calculation of the power spectral density from surface profile data," *Appl. Opt.* **34**, 201-208 (1995). [doi: 10.1364/AO.34.000201].
37. Velox CNC Specification Sheet.
38. M. Palmer, "Freeform Optics Fabrication and Post Processing," *Master Report* (2016).
39. Mach developers. (2003). *Using Mach 3 Mil-A user's guide to installation, configuration and operation*. Art Fenerty and John Prentice.
40. ZYGO, "Verifire™ Specification Sheet", <https://www.zygo.com/?/met/interferometers/verifire/>.
41. ZYGO, "Newview™ 8000 Specification Sheet" https://www.zygo.com/?/met/profilers/newview8000/&utm_source=AZO&utm_medium=referral&utm_content=NewView8000.